Available online at www.sciencedirect.com
ScienceDirect
Advances in Space Research 44 (2009) 494–500
ADVANCES IN SPACE RESEARCH (a COSPAR publication)
www.elsevier.com/locate/asr

A gravity wave analysis near to the Andes Range from GPS radio occultation data and mesoscale numerical simulations: Two case studies

P. Llamedo [a,*], A. de la Torre [a], P. Alexander [a], D. Luna [a], T. Schmidt [b], J. Wickert [b]

[a] Departamento de Fisica, Facultad de Ciencias Exactas y Naturales, Universidad de Buenos Aires, Ciudad Universitaria, 1428 Buenos Aires, Argentina
[b] Helmholtz Centre Potsdam, GFZ German Research Centre for Geosciences, Department 1: Geodesy and Remote Sensing, Telegrafenberg A17, Potsdam D-14473, Germany

Received 19 August 2008; received in revised form 25 February 2009; accepted 2 April 2009

Abstract

Global maps of potential wave energy per unit mass, recently performed with the Global Positioning System (GPS) Radio Occultation (RO) technique and different satellite missions (CHAMP and SAC-C since 2001, GRACE and COSMIC since 2006) revealed in Argentina, at the eastern side of the highest Andes Mountains, a considerable wave activity (WA) in comparison with other extra-tropical regions. The main gravity wave (GW) sources in this natural laboratory are deep convection (mainly during late Spring and Summer), topographic forcing and geostrophic adjustment.

The mesoscale numerical WRF (Weather Research and Forecasting) 2.1.2 model was used to simulate the atmospheric parameters during two representative RO events showing apparent intense WA in this region. The significance of the relative position of the RO lines of sight, the line of tangent points and GW phase surfaces during each event is discussed in relation with the apparent WA detected. The GPS RO technique may not be by itself reliable enough to quantify and locate WA of single events. Nevertheless, it should be considered a useful tool to observe the global WA from statistical studies. We also discuss the relative contribution of high and medium intrinsic frequency mountain waves regularly observed, coexisting with inertio gravity waves, their origin and propagation characteristics.
© 2009 COSPAR. Published by Elsevier Ltd. All rights reserved.

Keywords: Gravity waves; GPS RO; Andes; WRF

1. Introduction

The Argentine Mendoza region (roughly 70–65W, 30–40S) constitutes a natural laboratory where the main sources of gravity waves (GW) coexist. The Andes mountains represent a very important obstacle to the intense westerlies blowing from the Pacific Ocean, generating large amplitude GW. This North–South barrier (tops around 7 km) generates mountain waves (MW), whose phase surfaces are aligned nearly parallel to the mountains. These waves may be enhanced in the presence of an intense tropospheric jet that is usually present, avoiding possible critical level filtering. The possible generation of inertia gravity waves (IGW) by geostrophic adjustment near the permanent jet must be also considered. This process may take place when the wind evolution timescale becomes comparable to or shorter than the inertial period, which is around 1 day at 30S (e.g. Gill, 1982). Jet instabilities due to wind shear may alter the geostrophic equilibrium of the mean flow. The perturbed flow then relaxes to a new balanced state with redistribution of momentum, energy and potential vorticity and an additional radiation of excess energy as IGW. Downward/upward phase propagations above/below jets have been reported (Hirota and Niki, 1985).

* Corresponding author. Tel.: +54 11 45763300.
E-mail address: llamedo@df.uba.ar (P. Llamedo).

0273-1177/$36.00 © 2009 COSPAR. Published by Elsevier Ltd. All rights reserved.
doi:10.1016/j.asr.2009.04.023

The GPS RO (Global Positioning System Radio Occultation) technique gives valuable information about GW and their properties for a large part of the atmosphere. This method provides a global coverage, sub-Kelvin temperature accuracy, high vertical resolutions and long-term stability. These features and the absence of limitations from weather conditions make this technique unique (Kirchengast, 2004) and references therein. The obtained profiles have vertical resolutions progressively increasing from 0.5 km in the troposphere up to 1.4 km in the lower stratosphere (Kursinski et al., 1997) (nevertheless, the data are usually interpolated every 200 m) and a horizontal resolution about 150 km along each line of sight (LOS). The perigee of the LOS between satellites projected on the Earth's surface determines the geographical coordinates where the atmospheric parameters are given. Successive perigees during the occultation form the line of tangent points (LTP). The RO is sensitive to a certain portion of the full spectrum of horizontal and vertical wavelengths and depends on the relative orientation of the LOS and the wave vector to detect it (P. Alexander et al., 2008). Therefore, measured GW are affected by visibility effects of the observing instruments (Lange and Jacobi, 2003). For example, GW with horizontal wavelengths shorter than the horizontal resolution of GPS RO are frequently detected in the region we considered. This happens because LOS directions and constant wave surfaces due to MW have a predominant and nearly coincident North–South direction. Due to their similar measurement characteristics, all limb viewing techniques have a good vertical resolution and a coarse horizontal resolution and are thus sensitive to only a portion of the wavelength spectrum. Therefore, some of the conclusions drawn in this study for GPS RO may be extended to other instruments like LIMS, CRISTA, SABER and HIRDLS (Wu et al., 2006; M.J. Alexander et al., 2008).

Usually, GW activity can be quantified from GPS RO temperature profiles, by calculating the mean potential energy through the relative temperature variance content σ in a vertical column of air. For example, in de la Torre and Alexander (2005), this column was selected at a height interval $[z_1, z_2]$ above the tropopause:

$$\sigma = \frac{1}{(z_2 - z_1)} \int_{z_1}^{z_2} \left(\frac{\delta T}{T_B}\right)^2 dz \tag{1}$$

where δT and T_B are the band-pass filtered temperature perturbations between cutoffs at 3 and 9 km and the background temperature, respectively. MW in the geographic region studied in this paper usually have vertical wavelengths in this range. In the Southern Hemisphere, there are extratropical regions that exhibit a strong wave activity close to the Andes and to the Antarctic Peninsula which have been studied with limb sounding techniques (Ecker-

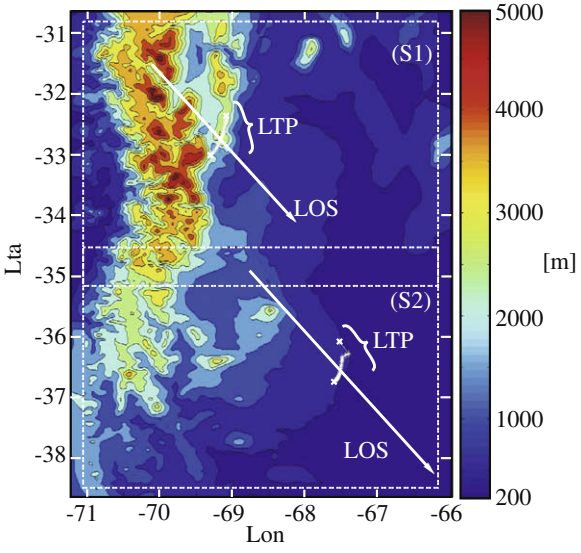

Fig. 1. Topography in the highest resolution domain for both simulations (S1 and S2) and the corresponding horizontal projections of LTP and LOS. Note that the LTP corresponding to S1 is situated almost over the highest Andes mountains whereas for S2 it is situated approximately 200 km east from the southern end of the mountain relief.

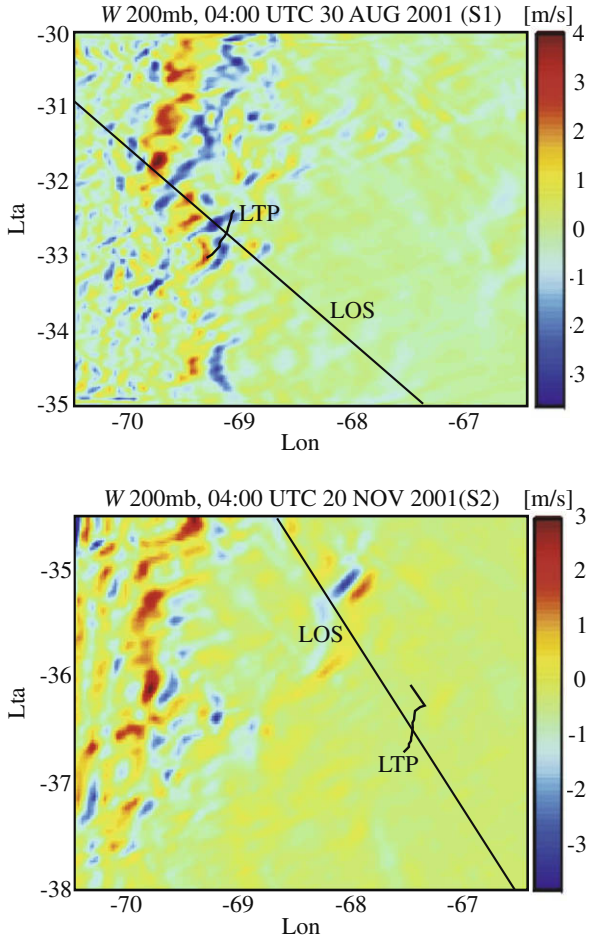

Fig. 2. Vertical velocity perturbation δW (m/s) at 200 mb and the time output closest to each RO event. Note that the largest amplitudes coincide with the highest mountains.

mann and Preusse, 1999; Jiang et al., 2002). Preusse et al. (2002) detected GW at 40–60S close to the Andes using the infrared limb sounding CRISTA instrument, confirmed by mesoscale model MM5 simulations. de la Torre et al. (2006) performed an analysis of the global distribution of gravity wave activity in the upper troposphere and lower stratosphere between June 2001 and March 2006, using GPS RO temperature profiles retrieved from the CHAMP satellite (Wickert et al., 2009). A significant WA with respect to other extra-tropical regions in the Southern Hemisphere was detected in Mendoza, Argentina, on the eastern side of the highest Andes mountains. We selected two events taking place in this location, showing intense WA. In order to evaluate the capability of the RO technique to quantify WA, we performed numerical simulations in both cases.

2. Mesoscale numerical results

Mesoscale models can simulate realistic GWs distributions in the troposphere and stratosphere and have been recently a major tool to study wave generation and propagation mechanisms (Zhang, 2004). Mesoscale models help to reveal detailed wave structures, energy sources, and possible maintenance mechanisms that are difficult to measure by satellite sensors. However, modeled GW properties and effects require observational verifications that are rarely available (Wu and Zhang, 2004).

We performed simulations with the WRF 2.1.2 model (Skamarock et al., 2005) during two SAC-C RO events showing a considerably intense WA (30 August 2001, 04:10 UTC and 20 November 2001, 03:58 UTC; hereinafter S1 and S2, respectively). In both cases, we employed three nested domains with effective horizontal grid spacing of 36, 12, and 4 km, respectively, and a time step equal to 30 s. The outer domains for S1 and S2 were limited, respectively, by the rectangles (74W, 27S, 55W, 38S) and (75W, 31S, 55W, 42S). The intermediate domains, respectively, are (73W, 28S, 62W, 37S) and (72W, 33S, 62W, 40S). The inner domains are shown in Fig. 1. The experiments were driven by assimilating lateral boundary conditions and sea surface temperatures from NCEP (National Centers for Environmental Prediction) reanalysis. The physical parametrizations already showed a reasonably good performance in simulating various characteristics of southern South America regional climatology. The simulations were initialized at least one day before the RO event in order to stabilize them. Typical westerlies are seen at and above 700 mb during both events. An intense jet core with zonal speed greater than 50 m/s is seen in both simulations at 250 mb. The jet core intensity varies more rapidly than the inertial period. Probable IGW radiated by geostrophic adjustment must then be considered.

Fig. 1 shows the topography in the highest resolution domain for both simulations. The horizontal projections of LTP and LOS corresponding to each RO event are

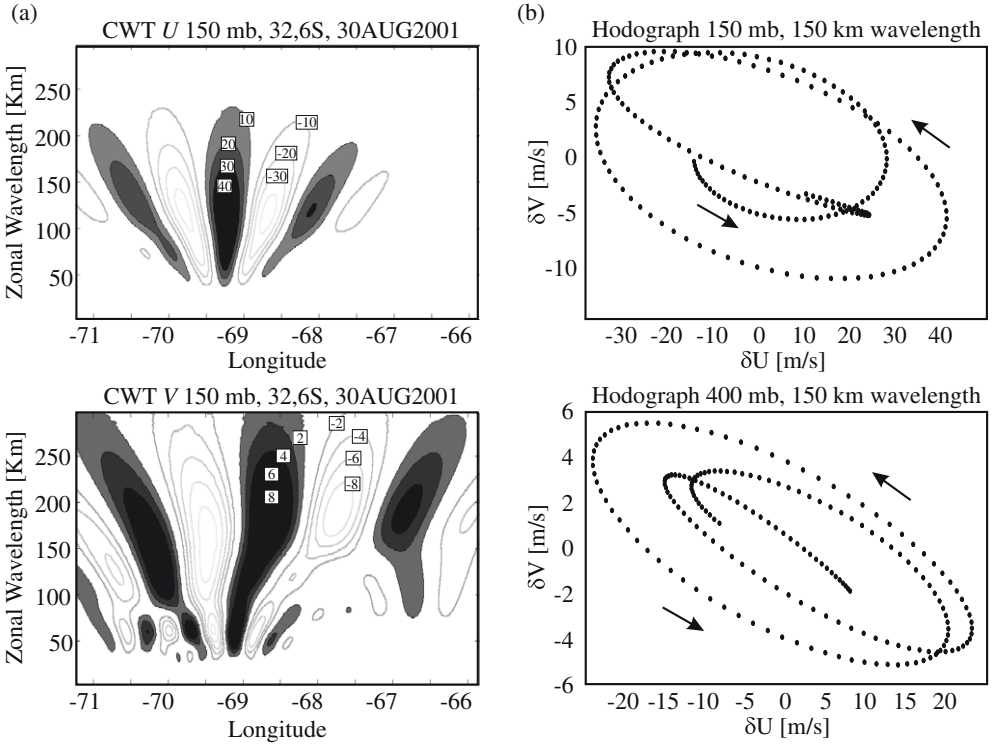

Fig. 3. (a) Morlet CWT for U (above) and V (below) at 32.6S, 150 mb and the time output closest to S1. Two principal modes were found both in U and V between 50 and 200 km. The origin of the horizontal axis coincides with the western limit of the domain (71W). (b) Hodograph at 150 mb (above) and 400 mb (below), for the longest wavelength component (see text).

shown. Note that the LTP corresponding to S1 is situated over the mountains whereas S2 is situated, on average, 200 km East of the mountains, over a plateau region. In both cases, the respective LOS are nearly parallel.

In order to study δT and the zonal, meridional and vertical velocity perturbations, δU, δV and δW, we first removed the background wind by employing a 2D filtering technique. A 10–550 km 2D band pass filter was applied to T, U, V and W, at each constant pressure level and time step. δW is recognized as an indicator of the presence of mountain wave activity (Shutts et al., 1988). Fig. 2 shows δW at 200 mb at the time output closest to each RO event. Both simulations reveal stationary mesoscale waves above the highest tops (≈500 mb), with constant phase surfaces quite parallel to the topography, suggesting their orographic origin. It is interesting to note that, even considering that RO temperature profiles reveal important WA for both events, the simulations evidence strong/weak δW variations (typically associated to mountain WA) in the vicinity of S1/S2 LTP. Possible GW contributions related to deep convection activity during both events were not supported by satellite imagery evidence.

As mentioned above, due to the rapidly varying jet core, long horizontal wavelength IGW radiated by geostrophic adjustment should also be considered. According to this, IGW with downward group velocity below the jet could be expected. We used continuous wavelet transform (CWT) (Torrence and Compo, 1998) to analyze wave parameters along different paths, at constant latitude and along the LOS direction, at different pressure levels and time steps. In every case, we found two principal wave modes in δU and δV situated at horizontal wavelengths between 50 and 200 km. In Fig. 3a, we can see the Morlet

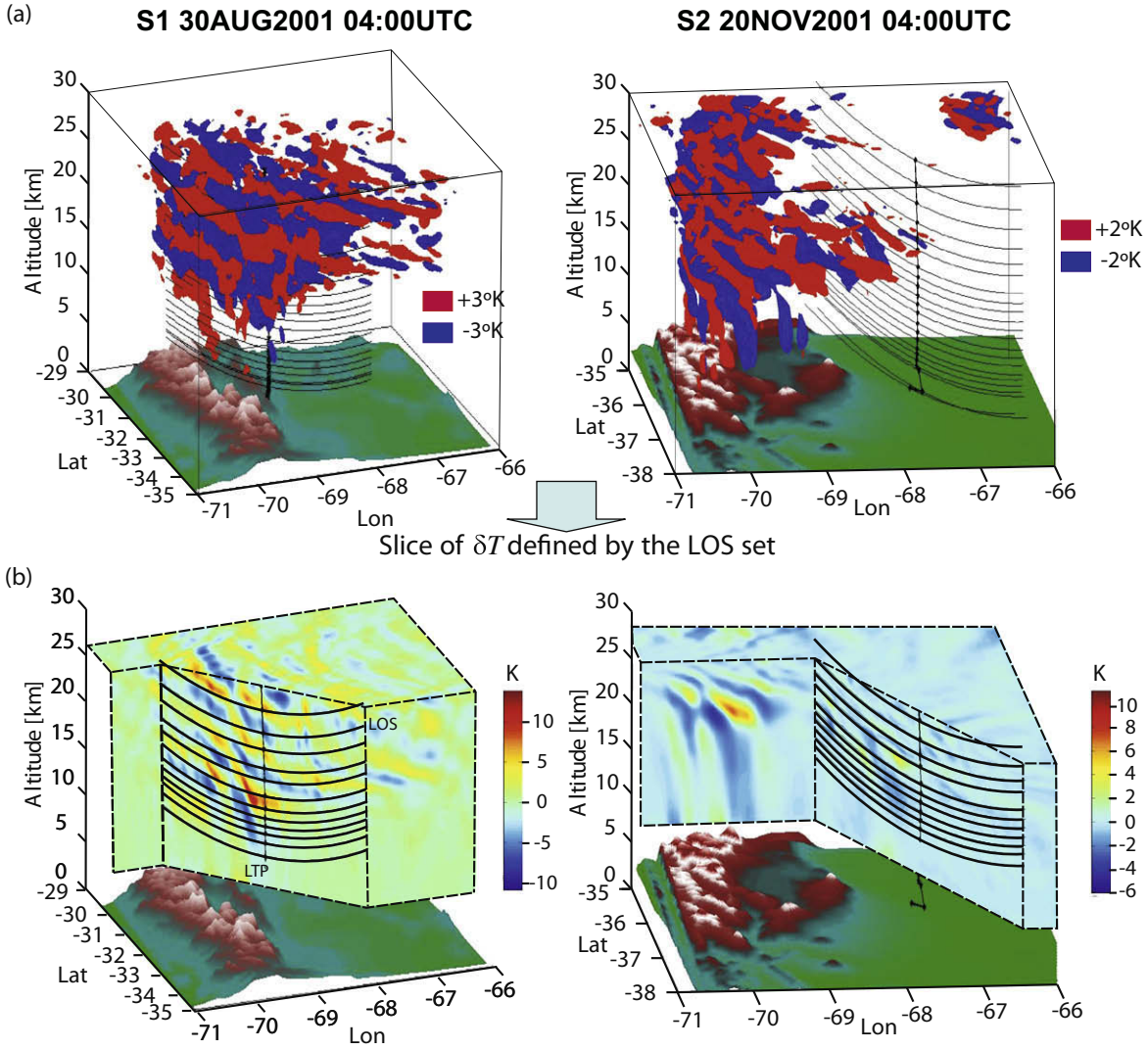

Fig. 4. (a) 3D view of the ±3 K δT contours for S1 and ±2 K δT contours for S2. Topography, LTP and LOS sets are also shown. (b) δT at the vertical cross section defined by the set of optical paths. Note that the optical ray in geographical coordinates is represented by a parabola rather than by a straight line. From (a) and (b), note the partial penetration of LOS into the high WA atmospheric region for S2.

CWT at a constant representative latitude (32.6S) and pressure level (150 mb), for S1.

Linear wave theory predicts an elliptic polarization relation between δU and δV for IGW. This means that the perturbation horizontal velocity vector $(\delta U, \delta V)$ rotates anticyclonically (counter-clockwise in the Southern Hemisphere) as one moves in a direction opposite to phase velocity (Gill, 1982). If the main wave source is at the ground and wave contributions from other sources are absent, the sense of rotation of $(\delta U, \delta V)$ does not change with height. When the source is located at a given altitude, energy is radiated at this level. In this case, the sense of rotation of $(\delta U, \delta V)$ must be different above and below this height. We may interpret each scale of the CWT as a band pass filter for this scale (wavelength). Fig. 3b shows the hodograph at 150 mb (above the jet) and 400 mb (below the jet) for the longest horizontal wavelength ($\lambda_H \approx 150$ km). Both hodographs rotate counter-clockwise eastwards at constant pressure level. This, together with the stationary phase surface slopes (see Fig. 4b), evidences a downward phase velocity (upward group velocity). We conclude that IGW do not stem from geostrophic adjustment and that the major source must be topographic forcing. This behavior is typical for winter and spring, when high stability conditions allow the propagation of large amplitude mountain waves.

The RO bending angle is an integrated weighted measure of the refractive index (and therefore temperature) in the atmosphere traversed by the optical ray. The contribution of the refractive index to the integral peaks at the perigee and decays exponentially away from it (P. Alexander et al., 2008). There is an uncertainty in the determination of the exact position of each tangent point (TP) in geographical coordinates. TPs may be displaced away from the perigee along each ray path, between ±25 km and ±50 km in the 10–16 km and 16–35 km altitude intervals, respectively (Liou et al., 2007). Due to these uncertainties, the peak of the exponential decay does not always coincide with each TP. This affects the horizontal resolution. Although the RO is an integrated weighted measure it is

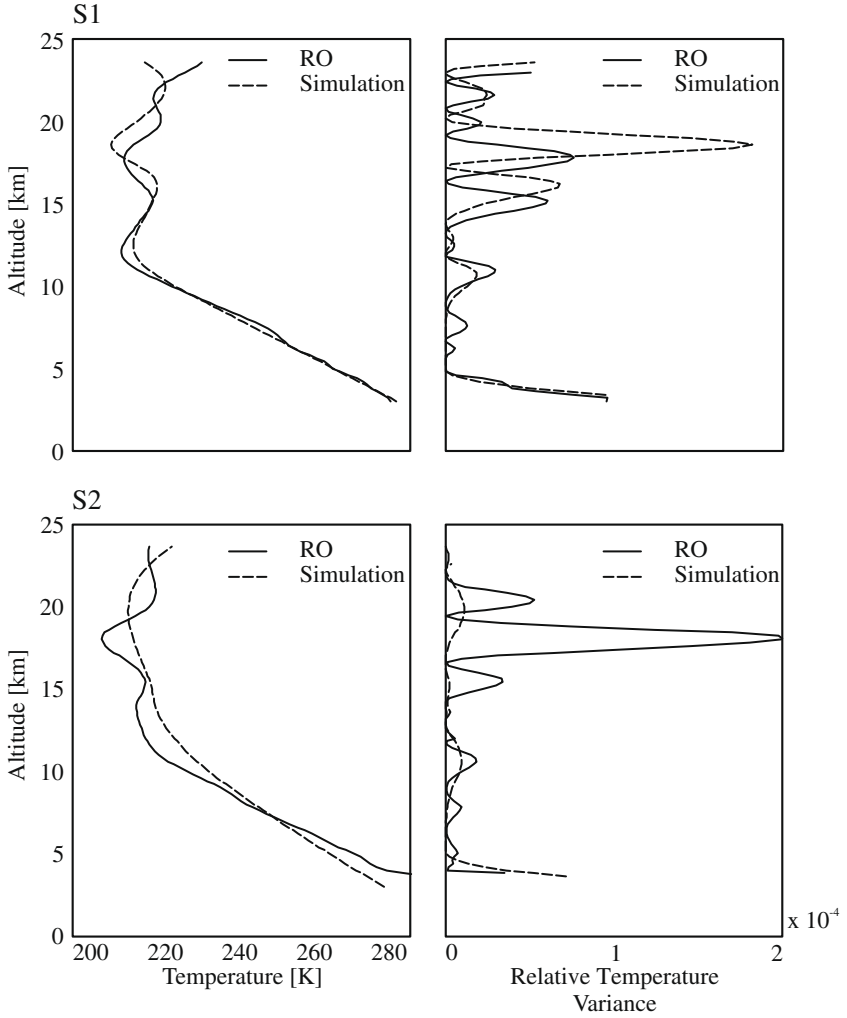

Fig. 5. Temperature profile (left) and the relative temperature variance (right) calculated from RO data and from simulation data (weighted integral measure along the LOS).

usually used as a point measure. In these cases, RO T profile indicate a magnified or even nonexistent WA at the perigees. This is the case in S2 (Fig. 4a and b, right), where each LOS penetrates a wave packet far away from its corresponding TP.

We must be careful about the atmospheric region where we detect intense WA. The proper interpretation must consider a few hundred kilometers around the TP. Fig. 4a shows δT at the vertical cross section defined by the set of LOS. Wave phase surfaces tilt westward, evidencing a downward–westward phase progression clearly corresponding to MW. Optical ray paths in the cross section are also shown. Note that each optical ray in geographical coordinates is represented by a parabola rather than by a straight line. Fig. 4b shows the 3D contours corresponding to $\delta T = \pm 3$ K for S1 and $\delta T = \pm 2$ K for S2. This plot includes LTP and LOS. A first insight shows an intense WA in S1 close to the tangent points (as predicted by the corresponding RO), whereas for S2, there are only weak wave packets in the troposphere, approximately 100 km away from the tangent points. Note in Fig. 4b for S2, just a partial penetration of LOS into the high wave amplitude atmospheric region. Fig. 5 shows the temperature profile and the relative temperature variance $((\delta T/T)^2)$ calculated from RO data and from simulation data (weighted integral measure along the LOS). As expected from Figs. 2 and 4, the RO T profile during S2 overestimates the WA. Taking into account these two examples, and the systematic GPS RO uncertainties mentioned above, a question arises: are these measurements adequate to quantify WA? It seems reasonable to think that GPS RO T data alone are not enough to quantify and locate WA of single events. At most, they provide a useful qualitative indication. Each event must be complemented with independent observations or with mesoscale simulations. However, we must keep in mind that the model results could tend to overstate the three dimensional wave field structure with respect to what actually occurs in this complex geographic region (Preusse et al., 2002). Notwithstanding these problems, it seems reasonable to draw statistical conclusions from the global WA distribution derived from GPS RO measurements, whenever a large number of T profiles is available.

3. Conclusions

We examined WRF results for two selected RO cases in a high WA region close to the Andes mountains. A wavelet analysis led us to identify two principal modes of oscillation with horizontal wavelengths between roughly 50 and 200 km, both clearly corresponding to mountain waves. A hodograph for the longest wave shows downward phase velocity at all heights of the simulation. This evidences that GW do not stem from geostrophic adjustment at jet levels, but from topographic forcing. We observe that one of the simulations does not show intense WA in the vicinity of the tangent points, even though the GPS RO temperature profile detects it. The GPS RO technique may not be by itself reliable enough to quantify and locate WA of single events. Nevertheless, it should be considered a useful tool to observe the global WA from statistical studies.

Acknowledgments

Manuscript prepared under Grants UBA X004 and CONICET PIP 5932. A. de la Torre and P. Alexander are members and P. Llamedo holds a fellowship of CONICET. We acknowledge data provided by the NOAA-CIRES/Climate Diagnostics Center and JPL (USA) and GFZ (Germany).

References

Alexander, M.J., Gille, J., Cavanaugh, C., et al. Global estimates of gravity wave momentum flux from high resolution dynamics limb sounder observations. J. Geophys. Res. 113, D15S18, doi:10.1029/2007JD008807, 2008.

Alexander, P., de la Torre, A., Llamedo, P. Interpretation of gravity wave signatures in GPS radio occultations. J. Geophys. Res. 113, D16117, doi:10.1029/2007JD009390, 2008.

de la Torre, A., Alexander, P. Gravity waves above Andes detected from GPS radio occultation temperature profiles: mountain forcing? Geophys. Res. Lett. 32, L17815, doi:10.1029/2005GL022959, 2005.

de la Torre, A., Schmidt, T., Wickert, J. A global analysis of wave potential energy in the lower stratosphere derived from 5 years of GPS radio occultation data with CHAMP. Geophys. Res. Lett. 33, L24809, doi:10.1029/2006GL027696, 2006.

Eckermann, S.D., Preusse, P. Global measurements of stratospheric mountain waves from space. Science 286, 1534–1537, 1999.

Gill, A. Atmosphere–Ocean Dynamics. Academic Press, New York, 1982.

Hirota, I., Niki, T. A statistical study of inertia-gravity waves in the middle atmosphere. J. Meteorol. Soc. Jpn. 63, 1055–1066, 1985.

Jiang, J.H., Wu, D.L., Eckermann, S.D. Upper Atmosphere Research Satellite (UARS) MLS observation of mountain waves over the Andes. J. Geophys. Res. 107, 8273, doi:10.1029/2002JD002091, 2002.

Kirchengast, G. Occultations for probing atmosphere and climate: setting the scene, in: Occultations for Probing Atmosphere and Climate. Springer, New York, pp. 1–8, 2004.

Kursinski, E.R., Hajj, G.A., Schofield, J.T., et al. Observing Earth's atmosphere with radio occultation measurement using the Global Positioning System. J. Geophys. Res. 102 (D19), 23429–23465, 1997.

Lange, M., Jacobi, Ch. Analysis of gravity waves from radio occultation measurements, in: First CHAMP Mission Results for Gravity, Magnetic and Atmospheric Studies. Springer, Berlin, pp. 479–484, 2003.

Liou, Y.A., Pavelyev, A.G., Liu, S.F., et al. FORMOSAT-3/COSMIC GPS radio occultation mission: preliminary results. IEEE Trans. Geo. Rem. Sens. 45, 3813–3826, 2007.

Preusse, P., Dörnbrack, A., Eckermann, S.D., et al. Space-based measurements of stratospheric mountain waves by CRISTA 1. Sensitivity, analysis method, and a case study. J. Geophys. Res. 107, 8178, doi:10.1029/2001JD000699, 2002.

Shutts, G.J., Kitchen, M., Hoare, P.H. A large amplitude gravity wave in the lower stratosphere detected by radiosonde. Q. J. R. Meteorol. Soc. 114, 579–594, 1988.

Skamarock, W.C., Klemp, J. B., Dudhia, J., et al. A Description of the Advanced Research WRF Version 2.NCAR Technical Note, 2005.

Torrence, C., Compo, G.P. A practical guide to wavelet analysis. Bull. Am. Meteorol. Soc. 79, 6178, 1998.

Wickert, J., Michalak, G., Schmidt, T., et al. GPS radio occultation: results from CHAMP, GRACE, and FORMOSAT-3/COSMIC. Terr. Atmos. Ocean. Sci. 20, doi:10.3319/TAO.2007.12.26.01 (F3C), 2009.

Wu, D.L., Preusse, P., Eckermann, S.D., et al. Remote sounding of atmospheric gravity waves with satellite limb and nadir techniques. Adv. Space Res. 37, 2269–2277, 2006.

Wu, D.L., Zhang, F. A study of mesoscale gravity waves over North Atlantic with satellite observations and a mesoscale model. J. Geophys. Res. 109, D22104, doi:10.1029/2004JD005090, 2004.

Zhang, F. Generation of mesoscale gravity waves in upper-tropospheric jet-front systems. J. Atmos. Sci. 61, 440–457, 2004.